

Shape-independent approximation for Bose-Einstein condensates interacting through a van der Waals potential

Barnali Chakrabarti¹ and Tapan Kumar Das²¹*Department of Physics, Lady Brabourne College, P-1/2 Surawardi Avenue, Calcutta-700017, India*²*Department of Physics, University of Calcutta, 92 A.P.C. Road, Calcutta-700009, India*

(Received 28 July 2008; published 16 December 2008)

We study the properties of Bose-Einstein condensates with the realistic van der Waals two-body interaction for large numbers of trapped atoms, solving the many-body Schrödinger equation by the potential harmonic expansion method. The effect of different C_6 parameters has been critically examined, starting from very few to 14 000 atoms to analyze and justify the idea of a shape-independent approximation. It is found that the condensate properties almost remain unchanged when the number of atoms are quite small (~ 100), in good agreement with earlier results of Blume and Greene [Phys. Rev. A **63**, 063601 (2001)], but we observe the appreciable effect of a long attractive tail when N is large, even in the low-density limit. The above reference considered only 20 atoms which is far from a real experimental situation. Our calculation gives a realistic scenario which justifies the use of a shape-dependent two-body interaction in many-body theories.

DOI: [10.1103/PhysRevA.78.063608](https://doi.org/10.1103/PhysRevA.78.063608)

PACS number(s): 03.75.Hh, 31.15.xj, 03.65.Ge, 03.75.Nt

I. INTRODUCTION

Most of the theoretical studies of inhomogeneous Bose gases use the shape-independent approximation (SIA), replacing the atom-atom interaction by a contact δ potential [1]. Dilute Bose-Einstein condensates (BEC) are known to possess the shape independence (SI) property, *viz.* observables of such condensates are independent of the functional shape of the two-body potential (2BP), corresponding to a particular value of the s -wave scattering length (a_s). This approximation is intuitively justified, since in a typical BEC, the atomic cloud is extremely dilute and the interparticle separation (~ 100 nm) is much larger than $|a_s|$ (typically ~ 1 nm). The validity criterion for this approximation is usually taken as $n|a_s|^3 \ll 1$, where n is the number density. Calculations testing SIA reported in the literature [2,3] deal mostly with condensates containing a relatively small number of atoms and standard short-ranged 2BP. Several mathematical shapes of 2BP have been tested. They range from a singular contact interaction [which corresponds to the Gross-Pitaevskii equation (GPE)] to the other extreme of smooth Gaussian-type potentials. The parameters of such potentials are so chosen as to result in the chosen value of a_s . Usually the potentials are chosen to be attractive or repulsive according to whether a_s is negative or positive, respectively. In the pseudopotential approximation the actual atom-atom potential is approximated by a δ function.

The actual interatomic potential has a strong repulsive core at a small separation and a deep attractive tail at large atomic separations. This is appropriately represented by the van der Waals potential with a hard core of radius r_c (HCvdW). In this paper, we critically examine SIA for a widely varying long-range tail of the 2BP, while a_s and the functional shape of the 2BP are kept unchanged. We choose the realistic HCvdW potential, for which the value of r_c has been adjusted to give the chosen value of a_s . We also investigate the effect of increasing particle number on the SIA.

The validity of the shape-independent approximation was first established by Bohn *et al.* [2], but it was only for three

trapped bosons, which is far from reality. By comparing the total ground-state energy in the Hartree-Fock theory with the exact ground-state energy, it has been shown [2] that the SIA is qualitatively good in the low-density limit. However the δ function interaction is not suitable as the correct two-body interaction in the configuration space. In another nice approach Blume and Greene [3] tested the validity of SIA using the essentially exact diffusion Monte Carlo (DMC) method. At the low-density limit, they established the SI picture convincingly, but deviations occur in high densities. They used only model short-range potentials and handled only up to 20 bosons.

The recent progress in creating atomic clouds with large dipole moment [4–7] initiates a growing interest with longer range interactions instead of taking only contact interaction. Even in the low-density limit the use of realistic interatomic potential in the many-body calculation has been emphasized by several authors [8,9]. The van der Waals potential is a good choice, as it properly takes care of the effect of electric dipole-dipole interaction due to induced polarization. Necessity of taking even longer range interactions such as $\frac{1}{r}$, $\frac{1}{r^3}$ or $\frac{1}{r^4}$ have also been pointed out [10–13].

In the present work, we consider pairs of neutral atoms (separation r_{ij}) interacting through

$$V(r_{ij}) = \infty \quad \text{for } r_{ij} \leq r_c \\ = -C_6/r_{ij}^6 \quad \text{for } r_{ij} > r_c, \quad (1)$$

where C_6 is the strength of the van der Waals interaction. Its value changes widely, by three orders of magnitude, from a small value for H atoms to a high value for Cs atoms [14]. It raises some important questions. First, will the shape-independence property be still valid for the wide range of C_6 parameters for a large number of bosons, even in the dilute regime? Second, how well the condensate properties will be reproduced in the GPE approach, for very large values of C_6 . Third, can we reconcile the realistic many-body result with the mean-field result?

So, in spite of some existing calculations with van der Waals potential [10,15], there remains a necessity of explicit and detailed study of actual condensates of alkali-metal atoms over a wide range of C_6 parameter and particle number. By calculating the ground-state energy and low-lying excitations, we find that the SI structure is still valid for the entire range of C_6 values chosen, when the number of bosons is quite small (≤ 100). In such cases, the condensate properties are in good agreement with both GPE and DMC results. As we increase the number of bosons in the trap, the results are significantly affected by the attractive tail (for the same a_s). Hence, for a larger number of atoms in the trap, we observe that the condensate energy does not strictly follow the SI property. Increasing C_6 gradually while keeping a_s fixed, we find that the condensate becomes gradually more attractive, although it remains quite stable even when particle number (A) is fairly large ($\sim 14\,000$). The relative change in energy compared to the GPE value, defined as $\mathcal{R}=(E_{\text{GPE}}-E_{\text{PHEM}})/E_{\text{PHEM}}$, gradually converges as A increases, for the entire range of C_6 values investigated.

We use our recently formulated many-body approach, called correlated potential harmonics expansion method (CPHEM) [16–19] to solve the A -body Schrödinger equation. For a particular chosen value of the C_6 parameter, we adjust (using an analytic relation [14]) the hard core radius, r_c , which will reproduce an experimental value of the s -wave scattering length, $a_s=0.004\,33$ oscillator unit (o.u.), corresponding to the original JILA experiment with ^{87}Rb atoms. Our calculation definitely makes a bridge between the shape-dependent interatomic potential used in the many-body picture with the shape-independent pseudopotential used in the GP equation.

In Sec. II, we introduce the methodology and the numerical techniques to tackle large number of trapped interacting bosons. Section III contains the results and discussions. Conclusions are drawn in Sec. IV.

II. METHODOLOGY

The Schrödinger equation in relative coordinates for a system of $A=N+1$ identical bosons, each of mass m , confined by an external isotropic harmonic oscillator of frequency ω , is

$$\left(-\frac{\hbar^2}{m} \sum_{i=1}^N \nabla_{\vec{\zeta}_i}^2 + \sum_{i=1}^N \frac{1}{2} m \omega^2 \zeta_i^2 + V_{\text{int}}(\vec{\zeta}_1, \dots, \vec{\zeta}_N) - E \right) \psi(\vec{\zeta}_1, \dots, \vec{\zeta}_N) = 0, \quad (2)$$

where $\{\vec{\zeta}_1, \dots, \vec{\zeta}_N\}$ is the set of N Jacobi vectors and V_{int} is the sum of all pairwise interactions. Hyperspherical harmonics expansion method (HHEM) is an essentially exact tool for many-body systems [20]. However, due to the very large degeneracy of the hyperspherical harmonics (HH) basis and complexity in the symmetrization of the wave function for large A [20,16], HHEM is practically restricted to $A=3$ only. Recently, we adopted the potential harmonics expansion method (PHEM) [21], which takes two-body correlations

into account, disregarding higher-body correlations. This is quite appropriate for dilute BEC, but convergence of the expansion basis is slow and the method is restricted to $A \sim 50$ [16,17]. We further developed it by including appropriate short-range correlations (CPHEM) in each Faddeev component [18,19]. It has already been established in our earlier works [18,19], that CPHEM is quite a powerful tool, especially for dilute condensates, and can handle a fairly large number ($A \sim 14\,000$) of bosons in a straightforward way. The method can also incorporate any realistic two-body interaction. The method is quite promising as we have successfully reproduced the experimental results, both for attractive and repulsive condensates, with good accuracy. In the following, we present a skeletal outline, which is needed for a clear reading. For the interested reader, we refer to our earlier works [16,18].

The many-body wave function is decomposed in Faddeev components,

$$\psi = \sum_{ij>i}^{N+1} \psi_{ij}. \quad (3)$$

The Faddeev component ψ_{ij} , corresponding to (ij) interacting pair, is a function of the pair separation \vec{r}_{ij} and the global length r (called hyperradius) only. We expand it in the potential harmonics (PH) [21] basis as

$$\psi_{ij}(\vec{r}_{ij}, r) = r^{-[(3N-1)/2]} \sum_K \mathcal{P}_{2K+l}^{lm}(\Omega_N^{(ij)}) \eta(\vec{r}_{ij}) u_K^l(r). \quad (4)$$

Here $\mathcal{P}_{2K+l}^{lm}(\Omega_N^{(ij)})$ is a PH [defined as the subset of hyperspherical harmonics (HH) basis needed for the expansion of $V(\vec{r}_{ij})$] and $\Omega_N^{(ij)}$ denotes the full set of hyperangles in $3N$ -dimensional space for the choice $\vec{\zeta}_N = \vec{r}_{ij}$, corresponding to the (ij) partition. The orbital angular momenta of the condensate and its projection are denoted by l and m , respectively. A short-range correlation function, $\eta(\vec{r}_{ij})$ is included, which simulates the short interacting pair separation behavior of the (ij) -Faddeev component, thereby enhancing the convergence rate of the expansion. It is obtained as the zero energy solution of the (ij) -pair relative motion in the chosen two-body potential

$$-\frac{\hbar^2}{m} \frac{1}{r_{ij}^2} \frac{d}{dr_{ij}} \left(r_{ij}^2 \frac{d\eta(r_{ij})}{dr_{ij}} \right) + V(r_{ij}) \eta(r_{ij}) = 0. \quad (5)$$

Substitution of Eqs. (3) and (4) in the many-body equation, Eq. (2) and projection on a PH for the (ij) partition gives rise to a set of coupled differential equations (CDE) in r ,

$$\left(-\frac{\hbar^2}{m} \frac{d^2}{dr^2} + V_{\text{trap}} + \frac{\hbar^2}{mr^2} [\bar{\mathcal{L}}(\bar{\mathcal{L}}+1) + 4K(K+\alpha+\beta+1)] - E \right) U_{Kl}(r) + \sum_{K'} \bar{V}_{KK'}(r) U_{K'l}(r) = 0, \quad (6)$$

where $\bar{\mathcal{L}}=l+\frac{3A-6}{2}$, $\alpha=\frac{3A-8}{2}$, $\beta=l+\frac{1}{2}$, and r dependence of $\bar{V}_{KK'}(r)$ is given by

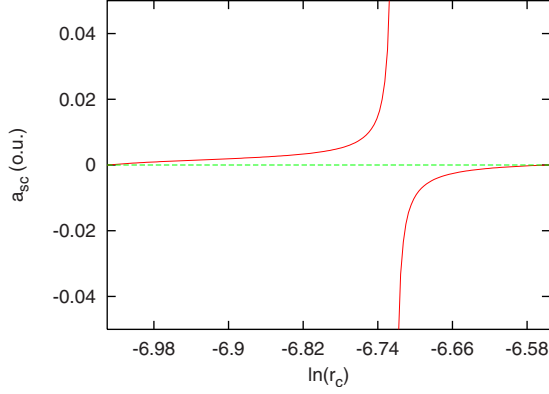


FIG. 1. (Color online) Plot of a_s against r_c (both in oscillator unit) for $C_6 = 6.489\,755 \times 10^{-11}$ oscillator unit.

$$\begin{aligned} \bar{V}_{KK'}(r) \propto & \int_{-1}^{+1} P_K^{\alpha\beta}(z) V\left(r \sqrt{\frac{1+z}{2}}\right) \\ & \times P_{K'}^{\alpha\beta}(z) \eta\left(r \sqrt{\frac{1+z}{2}}\right) w_l(z) dz, \end{aligned} \quad (7)$$

where $w_l(z)$ is the weight function of the Jacobi polynomial $P_K^{\alpha\beta}(z)$ [22]. The partial wave $U_{Kl}(r)$ is proportional to $u_K^l(r)$ [16].

Equation (6) is solved by the hyperspherical adiabatic approximation (HAA) [23], which assumes hyperradial motion to be slow compared to the hyperangular motion. The latter is solved by diagonalizing the potential matrix together with the diagonal hypercentrifugal repulsion for a particular value of r , whose lowest eigenvalue $\omega_0(r)$ is the effective potential in the hyperradial space, in which the collective motion of the condensate takes place. The energy and wave function of the condensate is obtained by solving the adiabatically separated hyperradial equation

$$\left(-\frac{\hbar^2}{m} \frac{d^2}{dr^2} + \omega_0(r) + \sum_{K=0}^{K_{\max}} \left| \frac{d\chi_{K0}(r)}{dr} \right|^2 - E \right) \zeta_0(r) = 0. \quad (8)$$

Here $\chi_{K0}(r)$ is the K th component of the column vector corresponding to the eigenvalue $\omega_0(r)$ and K values are truncated to K_{\max} subject to convergence in energy. Energy and wave function of the system are obtained by solving Eq. (8)

TABLE I. Ground-state energies by CPHEM (E_{CPHEM}) in o.u. for four different values of C_6 for $3 \leq A \leq 100$ atoms in Rb condensate ($a_s = 0.004\,33$). Values of C_6 are presented at the top of columns 3–6. For comparison GPE and available DMC results (from Ref. [3]) are also included.

A	C_6	E_{CPHEM}				E_{GPE}	E_{DMC}
		8×10^{-10}	8.5×10^{-11}	6.489755×10^{-11}	5×10^{-11}		
3		4.5103	4.5108	4.5103	4.5104	4.51032	4.51037
5		7.5342	7.5343	7.5345	7.5347	7.53432	7.53439
10		15.1530	15.1533	15.1544	15.1554	15.1534	15.1539
20		30.6385	30.6396	30.6438	30.6481	30.638	30.639
100		165.1177	165.1384	165.2272	165.3171	165.196	

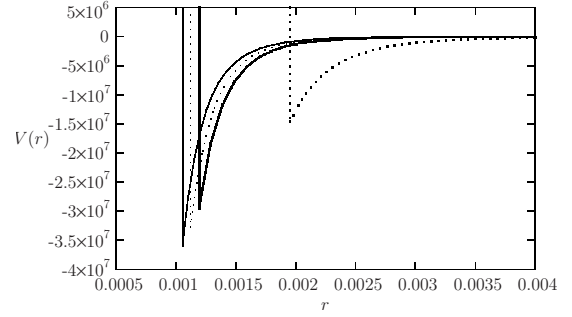


FIG. 2. Plots of two-body van der Waals potential for different C_6 parameters which give the same value of $a_s = (0.004\,33)$ oscillator unit. Value of C_6 (in oscillator unit) gradually increases towards the right-hand side: 5×10^{-11} , $6.489\,755 \times 10^{-11}$, 8.5×10^{-11} , 8×10^{-10} .

numerically. Partial wave $U_{Kl}(r)$ is given in HAA by $U_{Kl}(r) \approx \zeta_0(r) \chi_{K0}(r)$ [23].

III. RESULTS AND DISCUSSION

For the rubidium atoms the experimental value of C_6 is $6.489\,755 \times 10^{-11}$ o.u. [where “oscillator unit” (o.u.) corresponds to the JILA experiment [24]]. We vary C_6 , taking values both smaller and larger than the experimental one. When $C_6 \rightarrow 0$, the potential becomes a hard core one and r_c coincides with a_s . For a given value of r_c , a_s can be calculated by analytically solving Eq. (5) [14]. Figure 1 shows a plot of a_s versus $\ln(r_c)$, for the experimental C_6 . As r_c decreases from a large value, a_s decreases monotonically, until it passes through an infinite discontinuity (going from $-\infty$ to $+\infty$) at a particular value of r_c , with the potential just supporting a two-body bound state. Then the pattern repeats as r_c decreases further, with the appearance of an extra node (2BP supporting an extra bound state) in the zero-energy two-body wave function, for each additional infinite discontinuity. Similarly, for a fixed r_c , if C_6 is gradually increased, a_s will pass through infinite discontinuities, each time an extra node will appear in a two-body wave function.

To see how the condensate properties are affected by the strength of the long-range tail of the 2BP, we select three additional values of C_6 , in addition to the actual experimental value, one below and two above that value. They are (in

TABLE II. Dependence of ω_{0m} and r_m on C_6 for selected values of A .

A	$C_6=5 \times 10^{-11}$		$C_6=6.489755 \times 10^{-11}$		$C_6=8.5 \times 10^{-11}$		$C_6=8 \times 10^{-10}$	
	r_m	ω_{0m}	r_m	ω_{0m}	r_m	ω_{0m}	r_m	ω_{0m}
10	5.04	12.6411	5.04	12.6400	5.04	12.6309	5.04	12.6387
100	18.40	162.792	18.40	162.702	18.39	162.613	18.39	162.590
500	46.74	996.329	46.70	995.060	46.66	993.700	46.65	993.400
2000	113.97	5642.89	113.84	5631.14	113.71	5619.55	113.68	5616.85
10000	339.92	48792.7	339.47	48668.7	339.04	48546.3	338.93	48517.8
14000	428.81	77415.4	428.24	77214.8	427.68	77016.9	427.55	76970.8

o.u.): 5×10^{-11} , 6.489755×10^{-11} , 8×10^{-11} , and 8×10^{-10} , respectively. For each value of C_6 , we calculate corresponding r_c , such that a_s has the experimental value, *viz.* 0.00433 o.u. For each set of (C_6, r_c) , we solve the many-body equation for $A=3, 5, 20, \dots, 14000$ bosons. In the present picture, the condensate moves as a single quantum entity in the effective many-body potential $\omega_0(r)$ in the hyperradial space, corresponding to the collective motion of the condensate. $\omega_0(r)$ has the expected behavior, qualitatively similar to the noninteracting case; only it is shifted upward or downward depending whether the overall effect is repulsive or attractive. Also $\omega_0(r)$ is stiffer for smaller values of r . In the many-body picture, the effective potential behaves just like a one-dimensional potential in the hyperradial space, giving a tangible feeling for the experimental scenario of a trapped cloud. This differs from the picture presented by the GPE approach, which lacks the concept of an effective potential and one fails to visualize the physical picture.

To visualize the effect of different C_6 values on depth and range of the two-body potential, we plot $V(r_{ij})$ against r_{ij} for a few representative sets in Fig. 2. As C_6 increases, the attractive tail becomes more attractive, but simultaneously r_c also increases, although by a small amount, such that the net two-body attraction (volume integral) increases gradually. To quantify the effect of attraction we calculate the quantity $4\pi \int_{r_c}^{\infty} V(r)r^2 dr$. Its value changes from -0.01779 to -0.4541 , as we increase C_6 from 5×10^{-11} to 8×10^{-10} . Note, this

change occurs in each two-body pair. But kinetic and trap energies largely compensate this. Consequently the condensate energy decreases by a very small amount for small A . In the third through sixth columns of Table I we present the condensate ground-state energy for a small number of trapped bosons, *viz.* $A=3, 5, 10, 20, 100$. In the seventh column, we present the results obtained by solving the GP equation numerically [25]. Available DMC results from Ref. [3] are presented in the last column. One notices from Table I, that although increasing C_6 , the interatomic potential becomes more attractive, still the ground-state energies of the condensate are practically the same, for all the sets and also in very good agreement with both the GPE and the DMC results, for each value of A . Thus the many-body ground-state energy remains almost indistinguishable, indicating the validity of the SIA.

In the many-body calculation, the total condensate energy depends on the depth of the lowest eigenpotential, $\omega_0(r)$, and to a lesser extent on its stiffness near the minimum. In Table II, we present the position (r_m) and the value (ω_{0m}) of the minimum of $\omega_0(r)$ for selected values of A and for the chosen values of C_6 . The $\omega_0(r)$ curve changes very little, as C_6 changes by 16 times— ω_{0m} decreasing from 12.6411 o.u. to 12.6387 o.u. as C_6 increases from 5×10^{-11} to 8×10^{-10} , the position of the minimum remaining unchanged for $A=10$. Corresponding change in the minimum of $\omega_0(r)$ is 0.20 o.u. for $A=100$, while the position of the minimum still remains nearly unchanged. This small change

TABLE III. Total ground-state energy for four different C_6 parameters for $500 \leq A \leq 14000$ atoms. For comparison the GPE results are also presented.

A	C_6	E_{CPHEM}				E_{GPE}
		8×10^{-10}	8.5×10^{-11}	6.489755×10^{-11}	5×10^{-11}	
500		995.964	996.267	997.570	998.893	1033.70
1000		2319.86	2323.61	2327.60	2328.83	2424.36
2000		5619.45	5622.15	5633.73	5645.49	5880.76
4000		14030.9	14038.5	14071.0	14103.9	14653.6
6000		24211.8	24225.5	24284.1	24343.5	25233.0
8000		35780.7	35801.5	35890.2	35995.5	37236.2
10000		48520.4	48549.0	48671.3	48795.3	50414.1
12000		62286.9	62323.3	62482.1	62651.4	64648.8
14000		76973.4	77019.5	77217.4	77418.0	79823.8

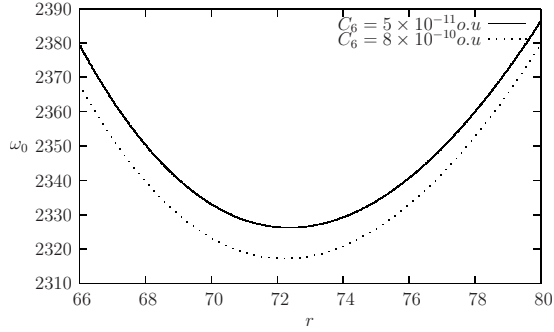


FIG. 3. Plot of lowest eigenpotential (in oscillator unit) against r (in oscillator unit) for 1000 bosons for two sets of C_6 parameters.

vis-à-vis a larger change in the two-body attraction is understood as follows. As C_6 increases, the total attractive interaction energy increases as $A(A-1)/2$, due to the shift of the 2BP (see Fig. 2), while trap energy and the kinetic energy increase as A . For smaller A , these two nearly balance. Hence, the effect of increasing C_6 on the ground-state energy of the condensate is negligible for small number of particles and the shape independence is well obeyed. The results for small A are also in good agreement with our earlier results using Gaussian-type model potentials [17,18]. However, the change in the minimum of $\omega_0(r)$ is quite appreciable when A increases. As A increases, the number of pairs, $A(A-1)/2$ increases rapidly and the net contribution from all pairs becomes appreciably negative and deviations from shape-independent property occurs. The results for larger A ($500 \leq A \leq 14000$) are presented in Table III. The ground-state energy gradually decreases with increase of C_6 , and strict shape independence is vitiated. In all cases, the many-body energy is lower than that by GPE. This is the effect of deep negative two-body potential and also the effect of two-body correlation, which lowers the ground-state energy, as discussed above. Although our results are lower than those of GPE, Table III shows the right limiting direction, as we gradually decrease the effect of the attractive tail, results are closer to the GPE values.

In Fig. 3, we plot the lowest eigenpotential [$\omega_0(r)$] of 1000 bosons for two extreme values of C_6 , *viz.* 5×10^{-11} o.u. and 8×10^{-10} o.u. The qualitative nature of

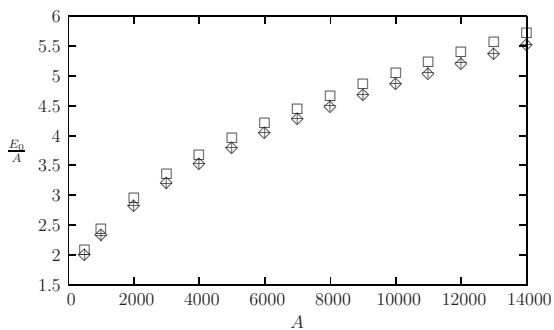


FIG. 4. Plot of ground-state energy (in oscillator unit) per particle as a function of A . The symbols are \diamond for $C_6=8 \times 10^{-10}$ oscillator unit; $+$ for $C_6=5 \times 10^{-11}$ oscillator unit, and \square for GP results.

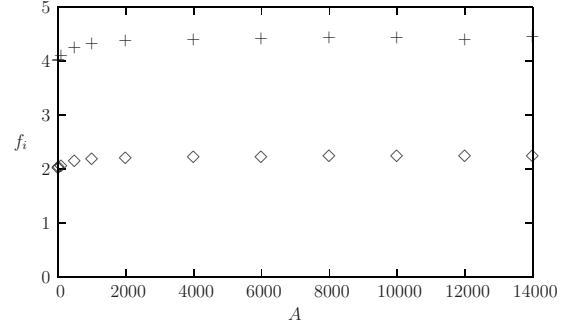


FIG. 5. Plot of the two lowest excitation frequencies ($f_i, i = 1, 2$) (in oscillator unit) for $C_6=5 \times 10^{-11}$ oscillator unit. The symbols are \diamond for f_1 and $+$ for f_2 .

$\omega_0(r)$ remains unchanged, but it is pushed downwards, making the condensate more attractive as C_6 increases. In Fig. 4, we plot the ground-state energy per particle against A for several C_6 values. The energy per particle is quite stable and shows the correct behavior. Making C_6 16 times larger, condensate energy per particle changes by 0.23% (for $A=500$) to 0.57% (for $A=14000$). In the same figure, we give GPE results, where energy per particle gradually increases with A , as in our case. In Fig. 5, the low-lying excitation frequencies for radial breathing modes $f_1=(E_1-E_0)$ and $f_2=(E_2-E_0)$ are plotted against A for $C_6=5 \times 10^{-11}$. In Table IV, we show the dependence of excitation frequencies on the C_6 parameter for several values of A . The results are seen to be fairly independent of C_6 . This means that as $\omega_0(r)$ becomes deeper, all the energy levels shift by approximately the same amount. Thus the “effective condensate potential” shifts as a whole without altering its shape.

Last, to compare the many-body results with those of GPE we define the quantity $\mathcal{R}=(E_{\text{GPE}}-E_{\text{PHEM}})/E_{\text{PHEM}}$ as the relative change in energy. In Fig. 6, we plot this quantity against A , for A ranging from 2000 to 14000, where the effect of C_6 is prominent. The lowest curve is for $C_6=5 \times 10^{-11}$. This implies that we belong to the correct C_6 limit. As one increases the C_6 parameter (making the condensate more attractive), the deviation from shape independence also increases as the curves are shifted upwards. However, they approach convergence as A increases. This is expected intuitively. By making the C_6 larger, the effect in the total ground-state energy is significant, however, this change will be distributed to all A , giving converging results when A is high. It has also been reflected in Fig. 4, where we see that $\frac{E_0}{A}$

TABLE IV. Low-lying excitation frequencies for two extreme values of C_6 parameters for $A=20, 100, 10000$.

A	C_6	5×10^{-11}	8×10^{-10}
20		2.026	2.0157
		4.031	4.0312
100		2.0479	2.0484
		4.0955	4.0962
10000		2.2209	2.2207
		4.4419	4.4415

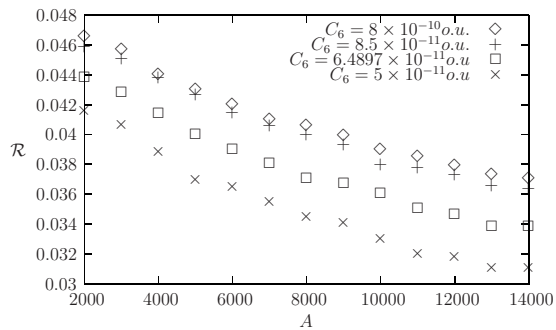


FIG. 6. Plot of the relative energy against particle number for different choices of C_6 parameters.

is close to GP value. It indicates that although the condensate becomes less repulsive as C_6 is increased, it remains quite stable (i.e., there is no collapse) even in the limit of large C_6 .

However, a close look at Fig. 6 shows that the quantity \mathcal{R} converges for large A . So in the usual BEC experiments which consider a large number of bosons (few millions) in the trap it is hard to detect the above correction to the ground-state energy. But in the recent experiments it is now possible to create a few-boson system. The alkali-metal atoms from a BEC reservoir are subjected to quantum tweezers and then further experiments are conducted in a number of squeezed states. The number-squeezed BEC is also created by “culling” atoms from a trapped condensate. Under such situation the effect of the many body can be observed experimentally where we see significant deviation in \mathcal{R} .

IV. CONCLUSION

In this work, we have critically examined the limits of validity of the shape independence approximation, used commonly in the study of dilute Bose-Einstein condensation. We have adopted the standard van der Waals interatomic potential and investigated the effect of increasing the

strength of the potential (i.e., the C_6 parameter), while the s -wave scattering length (a_s) is held constant to 0.00433 o.u.. It is found that the shape independent structure is well obeyed when the particle number (A) is less than about 100. For larger particle number, increase of C_6 reduces the ground-state energy by a small and asymptotically constant fraction. Our numerical results are in good agreement with earlier DMC calculations for a very few number of atoms in the trap, however substantial deviation occurs when A is quite high. As the previous calculations were restricted to only model type of potentials and also for very few atoms which is quite far from the experimental situation, it was necessary to study the universality of the shape-independent property in the aspect of a real experimental scenario. So our calculation is quite justified. Another important finding is how to make a bridge between the mean-field theory which used purely contact interaction and the many-body theory which uses realistic two-body interaction with finite range. The δ -function pseudopotential discusses the atomic interaction at the longest length scale, naturally the detailed description with shorter length scale [$\beta_6 = (\frac{2\mu C_6}{\hbar^2})^{1/4}$], which basically characterizes the long-range atomic interaction with $-\frac{C_6}{r^6}$ tail was necessary. Our results reflect the necessity of taking the shape-dependent two-body interaction in many-body calculations for a large number of bosons in the trap. The present experiments consider BEC with a large dipole moment, where one must include much longer range (compared to van der Waals) potential. Our present work definitely shows the way to handle finite range two-body interaction in many-body theory. The work in this direction is in progress.

ACKNOWLEDGMENTS

This work has been supported by Department of Science and Technology [Fund No. SR/S2/CMP/0059(2007) DST, India]. T.K.D. wishes to thank University Grants Commission (UGC, India).

-
- [1] F. Dalfovo, S. Giorgini, L. P. Pitaevskii, and S. Stringari, *Rev. Mod. Phys.* **71**, 463 (1999).
 [2] J. L. Bohn, B. D. Esry, and C. H. Greene, *Phys. Rev. A* **58**, 584 (1998).
 [3] D. Blume and C. H. Greene, *Phys. Rev. A* **63**, 063601 (2001).
 [4] S. Yi and L. You, *Phys. Rev. A* **61**, 041604(R) (2000).
 [5] K. Góral, K. Rzażewski, and T. Pfau, *Phys. Rev. A* **61**, 051601(R) (2000).
 [6] D. C. E. Bortolotti, S. Ronen, J. L. Bohn, and D. Blume, *Phys. Rev. Lett.* **97**, 160402 (2006).
 [7] K. Nho and D. P. Landau, *Phys. Rev. A* **72**, 023615 (2005).
 [8] B. Gao, *J. Phys. B* **36**, 2111 (2003), and references therein.
 [9] S. Geltman, *J. Phys. B* **37**, 315 (2004).
 [10] R. M. Kalas and D. Blume, *Phys. Rev. A* **77**, 032703 (2008).
 [11] A. Keles, S. Sevincli, and B. Tanatar, *Phys. Rev. A* **77**, 053604 (2008).
 [12] D. O’Dell, S. Giovanazzi, G. Kurizki, and V. M. Akulin, *Phys. Rev. Lett.* **84**, 5687 (2000).
 [13] S. Giovanazzi, G. Kurizki, I. E. Mazets, and S. Stringari, *Europhys. Lett.* **56**, 1 (2001).
 [14] C. J. Pethick and H. Smith, *Bose-Einstein Condensation in Dilute Gases* (Cambridge University Press, Cambridge, 2001).
 [15] B. Gao, *J. Phys. B* **37**, L227 (2004).
 [16] T. K. Das and B. Chakrabarti, *Phys. Rev. A* **70**, 063601 (2004).
 [17] B. Chakrabarti, A. Kundu, and T. K. Das, *J. Phys. B* **38**, 2457 (2005).
 [18] T. K. Das, S. Canuto, A. Kundu, and B. Chakrabarti, *Phys. Rev. A* **75**, 042705 (2007).
 [19] A. Kundu, B. Chakrabarti, T. K. Das, and S. Canuto, *J. Phys. B* **40**, 2225 (2007).
 [20] J. L. Ballot and M. Fabre de la Ripelle, *Ann. Phys. (N.Y.)* **127**, 62 (1980).
 [21] M. Fabre de la Ripelle, *Ann. Phys. (N.Y.)* **147**, 281 (1983).

- [22] M. Abramowitz and I. A. Stegun, *Handbook of Mathematical Functions* (Dover, New York, 1972), p. 773.
- [23] T. K. Das, H. T. Coelho, and M. Fabre de la Ripelle, Phys. Rev. C **26**, 2281 (1982).
- [24] M. H. Anderson *et al.*, Science **269**, 198 (1995).
- [25] R. P. Tiwari and A. Shukla, Comput. Phys. Commun. **174**, 966 (2006).